

# Many-Body Subradiant Excitations in Metamaterial Arrays: Experiment and Theory

Stewart D. Jenkins<sup>1</sup> and Janne Ruostekoski<sup>1</sup>

<sup>1</sup>*Mathematical Sciences and Centre for Photonic Metamaterials, University of Southampton, Southampton SO17 1BJ, United Kingdom*

Nikitas Papasimakis,<sup>2</sup> Salvatore Savo,<sup>2,3</sup> and Nikolay I. Zheludev<sup>2,4</sup>

<sup>2</sup>*Optoelectronics Research Centre and Centre for Photonic Metamaterials, University of Southampton, Southampton SO17 1BJ, United Kingdom*

<sup>3</sup>*TetraScience Inc., 114 Western Ave, Boston, Massachusetts 02134, USA*

<sup>4</sup>*Centre for Disruptive Photonic Technologies, School of Physical and Mathematical Sciences and The Photonics Institute, Nanyang Technological University, Singapore 637378, Singapore*

(Received 31 October 2016; published 3 August 2017)

Subradiant excitations, originally predicted by Dicke, have posed a long-standing challenge in physics owing to their weak radiative coupling to environment. Here we engineer massive coherently driven classical subradiance in planar metamaterial arrays as a spatially extended eigenmode comprising over 1000 metamolecules. By comparing the near- and far-field response in large-scale numerical simulations with those in experimental observations we identify strong evidence for classically correlated multi-metamolecule subradiant states that dominate the total excitation energy. We show that similar spatially extended many-body subradiance can also exist in plasmonic metamaterial arrays at optical frequencies.

DOI: [10.1103/PhysRevLett.119.053901](https://doi.org/10.1103/PhysRevLett.119.053901)

The classic example of neutrons and magnetic dipole radiation by Dicke [1] over 60 years ago describes the collective super-radiant and subradiant response of emitters at high density. Super-radiance, where the emission is enhanced due to constructive interference, has been experimentally observed in a variety of systems [2]. For subradiant states the emission is suppressed owing to the destructive interference of the radiation from the emitters. Because of the inherently weak coupling of the subradiant states to external electromagnetic (EM) fields, their experimental studies have been limited. In the early experiments subradiant emission was observed for two trapped ions [3] as well as for two trapped molecules [4]. Two-particle subradiant and super-radiant states have an analogy with the gerade (even) and ungerade (odd) symmetry states of homonuclear molecular dimers, and subradiant states have also been created in weakly bound ultracold Sr<sub>2</sub> [5] and Yb<sub>2</sub> [6] molecules. Super-radiant states in dimers represent excitations via strong electric dipole transitions, while subradiant states may, e.g., be produced by weak magnetic dipole or electric quadrupole transitions.

Similar effects have been investigated in the context of plasmonics, where the analogy between nanostructured plasmonic resonators and molecular states encountered in natural media has led to a plasmon hybridization theory [7]. Excitations in such systems, reminiscent of molecular wave functions, have consequently resulted in an analysis of dark and bright modes, with subradiant and super-radiant characteristics, respectively. Narrow Fano resonances in the transmitted field or subradiant and super-radiant excitations were experimentally observed in plasmonic resonators

consisting of three or four nanorods [8,9], and in plasmonic heptamers [10–12], while efforts to increase the mode complexity of the resonators are attracting considerable attention [13,14]. Recent theoretical work also highlighted that the connection between transmission resonances and the existence of subradiant excitations is less obvious than commonly recognized, since narrow Fano resonances are also produced by the interference of nonorthogonal modes even in the absence of subradiance [15,16].

Experiments on EM field transmission in large planar metamaterial arrays demonstrated narrow spectral features and changes in the resonances due to the nature of the resonators or the size of the system [17,18]. Such findings point toward a possible existence of subradiant excitations, and here we provide a detailed analysis of “coherent” planar metamaterial arrays that link the near- and far-field observations of the resonance behavior to large-scale numerical simulations of a microscopic theory of EM-field-mediated resonator interactions. We provide strong evidence that the observed resonance features in the reflection spectra directly correspond to the excitation of a single subradiant eigenmode spatially extending over the entire metamaterial lattice of over 1000 unit-cell resonators, or metamolecules. The results therefore rule out other possible explanations [15,16] of the narrow resonances as well as potential incoherent sources of suppressed radiation, such as radiation trapping [19,20], and also provide a *post facto* demonstration for the existence of subradiance in [17,18]. Rather surprisingly, we find that the created *multimetamolecule* subradiant state can confine 70% (for the plasmonic case 60%) of the total excitation of the array. Consequently, our analysis demonstrates the existence

of coherent and correlated many-body subradiant excitations that dramatically differ from subradiant modes restricted to a single individual metamolecule. The work not only provides a controlled environment for the study of many-body subradiance, but also a platform that can potentially be exploited, e.g., in high-precision measurements, metamaterial-based light emitters [21,22], spectral filters [23], imaging [24], and nonlinear processes [25].

We consider metamaterial planar arrays consisting of asymmetric split-ring (ASR) metamolecules formed by two discrete circular arcs [or meta-atoms; see Fig. 1(a)] [17,18,26]. Each ASR in the array, labeled by index  $\ell$  ( $\ell = 1, \dots, N$ ), can have a symmetric mode ( $\ell, +$ ), with the currents in the two arcs oscillating in phase, and an antisymmetric mode ( $\ell, -$ ), with the currents oscillating  $\pi$  out of phase. The symmetric mode produces a net electric dipole in the array plane and the antisymmetric mode a net magnetic dipole normal to the plane (accompanied by a weaker electric quadrupole moment). If the two arcs were symmetric, we would have a symmetric split-ring (SSR) resonator, and ( $\ell, \pm$ ) would form the metamolecule eigenfunctions. These modes display classical analogy to the wave functions of a homonuclear dimer molecule, such that the subradiant gerade and the super-radiant ungerade states are reminiscent of ( $\ell, -$ ) and ( $\ell, +$ ), respectively [27]. The metamolecules respond as linear classical harmonic oscillators, driven by a coherent field, and are therefore different from two-level entangled single-excitation molecules or strongly driven nonlinear quantum states [28]. However, two-level systems, such as atoms, also behave as classical harmonic oscillators in the low light intensity limit when driven by a field in a coherent state [29,30], illustrating the generality of the phenomenon across different physical systems [27].

The ASR asymmetry couples the two modes ( $\ell, \pm$ ), such that both of them can, in principle, be excited by driving only one of them with incident EM fields (depending on the frequency, propagation direction, etc.). For an incident plane wave that propagates along the normal to the

lattice couples directly only to the electric dipoles of the ( $\ell, +$ ) mode, since the magnetic dipoles point along the propagation direction. If the magnetic dipole radiation of the ( $\ell, -$ ) mode is much weaker than the electric dipole radiation of ( $\ell, +$ ), the asymmetry-induced coupling between broad and narrow resonance modes shows up as a characteristic Fano resonance in the transmission spectrum. However, in experimental situations the dipole radiation rates are comparable and no Fano resonance can be identified for a single ASR metamolecule [17]. However, interactions between the resonators, mediated by scattered fields, can have a profound impact. In extreme cases the radiative interactions can lead to correlations between the excitations that are associated with recurrent scattering processes [29,38–42] in which a wave scatters more than once by the same resonator.

The collective response of ASR arrays is investigated by performing large-scale numerical simulations. We use the same general formalism as previously, with the details reported elsewhere [31] and only a brief recap here [27]. Each meta-atom  $j$  is represented by a single mode of current oscillation that behaves as an effective *RLC* circuit with resonance frequency  $\omega_j$ . Each meta-atom is treated in the point dipole approximation with an in-plane electric dipole  $\mathbf{d}_j(t)$  and a perpendicular magnetic dipole  $\mathbf{m}_j(t)$ ; see Fig. 1. The electric and magnetic dipole moments of the meta-atoms radiate at the rates  $\Gamma_e$  and  $\Gamma_m$ , respectively. We also add a nonradiative loss rate  $\Gamma_o$ , such that the total decay rate of the meta-atom excitations is  $\Gamma = \Gamma_e + \Gamma_m + \Gamma_o$ . In the metamaterial array a meta-atom is driven by the sum of the incident fields and the fields scattered by all the other meta-atom resonators in the system. The meta-atom then acts as a source of radiation that, in turn, drives the other meta-atoms. This leads to a coupled set of equations between the meta-atom excitations that describe the EM field mediated interactions and allow us to evaluate the normal mode excitations of the system. This EM coupling between metamolecules leads to the emergence of many-body effects in the response of the metamaterial.

The experimental setup is described in detail in [43]. The measurements were performed on periodic metamaterial arrays of metallic ASR resonators. The asymmetry is introduced by a difference in length of the two arcs, corresponding to angles  $160^\circ$  and  $140^\circ$ . This results in the different resonance frequencies of the two arcs  $\omega_0 \pm \delta\omega$ , where  $\omega_0$  would be the resonance frequency of one arc in a SSR metamolecule. The far-field characterization of the metamaterial arrays was performed in an anechoic chamber with broadband linearly polarized antennas at normal incidence. Near-field mapping of the metamaterial samples was performed in a microwave scanning near-field microscope [43]. Following the fabricated sample, the simulated microwave metamaterial array in a steady-state response comprised  $30 \times 36$  unit cells with a lattice spacing of  $a = 0.28\lambda \approx 7.5$  mm ( $\lambda = 2\pi c/\omega_0$ )

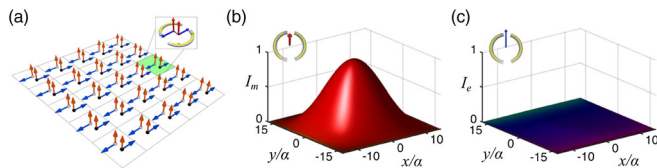


FIG. 1. (a) A schematic illustration of the planar metamaterial array consisting of asymmetric split-ring metamolecules. Each metamolecule has two constituent circuit resonator arcs, or meta-atoms, whose out-of-phase oscillating currents produce a strong net magnetic dipole perpendicular to the array. The arrows on the plane (blue arrows) represent the electric dipole of each arc and the arrows normal to the plane (red arrows) represent the magnetic dipoles generated by pairs of arcs. In a collective pure phase-coherent magnetic (PM) mode all magnetic dipoles in the array oscillate in phase. [(b) and (c)] Numerically calculated magnetic dipole (b) and electric dipole (c) excitation profiles for this mode.

assuming  $\Gamma_e = \Gamma_m$  and  $\delta\omega = 0.3\Gamma$ . Any losses in the metamaterial are almost solely due to the supporting substrate, as metals at low frequencies (GHz) exhibit negligible dissipation loss. These were incorporated by setting  $\Gamma_o = 0.07\Gamma$  that also provided the best fitting to the collective experimental response. In order to model the effects of the nonuniform illumination in the response of the array, we input the experimentally measured incident field profile in the numerical calculations.

In Fig. 2(a) we show a side-by-side comparison for the far-field measurements and numerical calculations of the reflected field intensity spectrum in a narrow cone in the back direction. The spectral response of the metamaterials exhibits a narrow Fano resonance [26] associated with the magnetic dipole excitation of the metamolecules. Numerical calculations are in good qualitative agreement with the experimental observations, indicating that the model captures well the multiple scattering phenomena between the resonators. Although an isolated ASR metamolecule exhibits no sharp resonance, the large array of interacting metamolecules displays a high-quality *collective* resonance. The resonance results entirely from interactions between the metamolecules that are mediated by the scattered fields. This is illustrated in Fig. 2(b), where we show the calculated spectra of weakly and noninteracting metamolecules of the same array, illustrating how an increased spatial separation leads to a substantially less pronounced, broader resonance.

The origin of these resonances can be traced to the eigenmodes of the metamaterial array. In particular, a uniform incident field normal to the lattice plane would couple most strongly to collective modes where metamolecules oscillate in phase, which is the case for a pure phase-coherent electric (PE) and a pure phase coherent magnetic (PM) dipole mode. For a SSR array these are collective eigenmodes of the system, similarly as the  $(\ell, \pm)$  modes are eigenstates of a single SSR metamolecule. The

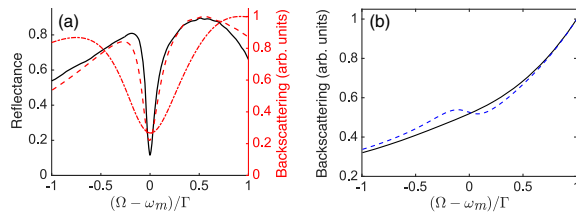


FIG. 2. (a) Experimentally measured reflectance (black line) and numerically calculated back-scattered intensity (red dashed line) spectra from a  $30 \times 36$  ASR microwave metamaterial array with a lattice spacing of  $a = 0.28\lambda$ . We also show calculated spectra (red dash-dot line) for arrays of plasmonic resonators ( $a = 0.2\lambda$ ). (b) Calculated spectra from microwave arrays of noninteracting metamolecules (black line), and arrays with a large lattice spacing of  $a = 1.9\lambda$  (dashed blue line) and thus weakened interactions. The frequencies are in the units of the single arc decay rate  $\Gamma$ , centered at the resonance frequency  $\omega_m$  of the phase coherent magnetic eigenmode of the corresponding SSR array.

PM mode of the studied case is shown in Fig. 1(b). Owing to the asymmetry of the ASR arcs, PE and PM modes in the ASR metamaterial array are no longer eigenmodes and are coupled by the asymmetry. The role of the different modes can be quantified by analyzing the collective eigenmodes of the strongly coupled resonator array. In Fig. 3(a) we show the overlap between the PE and PM modes and the steady-state excitation responsible for the far-field spectrum of Fig. 2(a). Here the overlap measure between an eigenmode  $\mathbf{v}_j$  with an excitation  $\mathbf{b}$  is defined by  $O_j(\mathbf{b}) \equiv |\mathbf{v}_j^T \mathbf{b}|^2 / \sum_i |\mathbf{v}_i^T \mathbf{b}|^2$ , where the summation runs over all the eigenmodes. Since the incident field in the experiment is not uniform, the coupling can drive strongly also other modes than PE and PM modes. However, the numerical results indicate that both PM and PE modes still play a significant role in the response of the metamaterial. PM mode excitation constitutes 63% of the total excitation at the resonance and rapidly decays outside of it. PE excitation is notable only outside of the resonance. The most remarkable feature is the very strongly subradiant nature of the PM mode; we find that in the corresponding SSR array, where the symmetry between the arcs of the metamolecules is not broken and where the PM mode is an eigenmode, its radiative decay rate would only be about  $\gamma_m \approx 0.011 \Gamma$  (together with the nonradiative Ohmic loss rate, the total decay rate is still only  $0.081 \Gamma$ ). For the PE mode the total decay rate in the corresponding SSR array would be about  $\gamma_e \approx 3.0 \Gamma$ , indicating super-radiant decay. In the ASR array, the asymmetry between the ASR arcs couples PE and PM modes. Hence, the Fano resonance at the frequency  $\omega_m$  (the resonance frequency of the PM mode) results from the interference between the collective

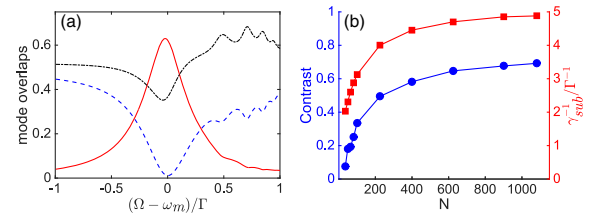


FIG. 3. (a) The contribution of a pure phase-coherent magnetic (PM; solid red line), pure phase-coherent electric (PE; dashed blue line) mode, and all the other eigenmodes of the symmetric system (dash-dot black line) to the steady-state excitation of the spectrum in Fig. 2(a). The phase-coherent magnetic dipole mode is dominant at the Fano resonance, while the phase-coherent electric dipole mode is significantly excited only outside the resonance. (b) The dependence of the Fano resonance depth [defined as  $c = (I_{\max} - I_{\min})/I_{\max}$ , where  $I_{\min}$  is the minimum reflected intensity on resonance, and  $I_{\max}$  is the reflected intensity at the lesser of the adjacent local maxima; blue line] and inverse linewidth,  $\gamma_{\text{sub}}^{-1}$ , of the dominant subradiant eigenmode of the array (red line) on the size of the metamaterial array,  $N$ . In the absence of the Fano resonance  $c = 0$ , while  $c = 1$  implies full reflection at the resonance frequency.

subradiant PM mode with an extremely narrow radiative linewidth and the super-radiant PE mode. The general behavior of the PM and PE modes is consistent with their radiation patterns. The dipoles aligned in the plane in the PE mode strongly reflect EM fields normal to the plane, while the PM mode dipoles emit into the plane of the lattice and suppress reflection.

So far we have described the ASR metamaterial response in terms of PM and PE modes that are not eigenmodes in the ASR array. In order to show that we have prepared subradiant many-body excitations we calculate the eigenmodes of the ASR array [27]. For a linear system, these also determine the dynamics and the decay of a radiative excitation amplitude satisfying  $\sum_j b_j \exp(i\delta_j t - \gamma_j t)$ , where  $\gamma_j$ ,  $\delta_j$ , and  $|b_j|^2$  are the collective eigenmode linewidths and line shifts, and the occupation estimates. After the incident field is turned off, the modes with broad resonances decay fast, and we are only left with the long-living subradiant modes. We find that the steady-state excitation at the Fano resonance is overwhelmingly dominated (close to 70% of the total excitation) by a subradiant eigenmode with the decay rate of  $\gamma_{\text{sub}} \approx 0.21 \Gamma$  and the resonance frequency  $\omega_{\text{sub}} \approx \omega_m - 0.017 \Gamma$ . Remarkably, this subradiant excitation is a correlated many-body excitation between a large number of metamolecules and extends over the entire metamaterial lattice. This is illustrated in Fig. 3(b), where we show the numerically calculated dependence of the radiative linewidth of the eigenmode on the size of the array. In Fig. 3(b) we approximately maintain the aspect ratio of the array while changing the number of metamolecules from 1 to the experimental value of 1080. The increase in the number of resonators notably continues reducing the linewidth even in the case of over 1000 metamolecules (over 2000 meta-atoms). Figure 3(b) also shows how the far-field resonance properties are directly linked to the radiative resonance linewidth of the subradiant excitation by comparing the resonance contrast with the eigenmode linewidth; we observe notably similar profiles for the emergent resonance and the subradiant mode linewidth as a function of the number of metamolecules, indicating that both result from the same collective interaction phenomena, ruling out single-particle interference effects, similar to electromagnetically-induced transparency [44]. The transmission resonance through an ASR array and its narrowing as a function of the size of the system has been previously experimentally observed [18]. The emergence of the Fano resonance implies a coupling between modes with a broad and a narrow resonance. Although this does not necessarily indicate the existence of subradiance in the system, our detailed theoretical and numerical comparisons provide strong evidence of correlated many-body multimetamolecule subradiant excitations of distant metamolecules that spatially extend over the entire metamaterial lattice.

In Fig. 4 we show near-field measurements of the microwave radiation of the array at the Fano resonance and the corresponding theoretical calculation. Using the

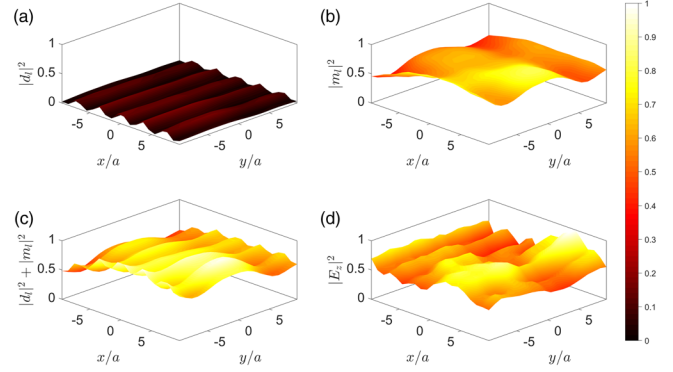


FIG. 4. Numerically calculated [(a)–(c)] and experimental (d) near-field excitations of a microwave metamaterial array at the transmission peak: (a) electric  $|d_e|^2$  and (b) magnetic  $|m_e|^2$  dipole intensity, (c) total excitation  $|d_e|^2 + |m_e|^2$ , and (d) experimentally measured electric field intensity.

experimentally measured nonuniform incident field profile, the numerical model qualitatively captures the characteristic striplike feature of the near-field excitation along the axis of the ASR arcs, but underestimates the nonuniformity of the excitations. In the theoretical model we also analyze the separate contributions of the magnetic and electric dipole excitations. The striplike pattern is identifiable only in the electric dipole excitations, but also the near field displays the concentration of resonant excitation on the magnetic dipoles and PM mode.

One may ask whether a similar multimetamolecule subradiant excitation can be observed also in plasmonic metamaterials in the optical domain, where Ohmic losses in metals are higher than at microwave frequencies. In plasmonic resonators the stronger Ohmic losses result in absorption of light and suppress the long-range light-mediated interactions between the different metamolecules. By performing numerical simulations for a plasmonic ASR array in the optical domain using realistic parameters we found that suitable parameter regimes for strong collective effects can also be found for plasmonic systems when the radiative decay is sufficiently strong ( $Q$ -factors of individual resonators are sufficiently low). One can show that a cooperative resonance is especially pronounced if the asymmetry that drives the subradiant mode also satisfies  $\delta\omega^2 \gg \gamma_m \gamma_e$ , requiring large  $\delta\omega$  when the nonradiative losses are substantial. For instance, we take  $\Gamma_o = 0.25 \Gamma$  that is comparable with those observed for Fano resonance experiments on gold rods [8] and obtained by Drude-model-based estimates [32]. The results for asymmetry  $\delta\omega = 0.75 \Gamma$  and lattice spacing  $a = 0.2\lambda$  are displayed in Fig. 2(a) that clearly show the existence of the resonance in the far-field spectrum. The resonance is broader than in the microwave case, but still includes a strong contribution from the PM mode ( $\sim 45\%$ ), whereas the PE mode is at a minimum (2.5%) [27]. We also calculated the ASR eigenmodes, and at the exact resonance  $\sim 60\%$  of the excitation is confined in a subradiant eigenmode with the

linewidth of  $\gamma_{\text{sub}} \approx 0.75 \Gamma$ , indicating a dominant collective subradiant excitation in the system. (In the corresponding SSR system the resonance linewidths of PM and PE modes would be  $\gamma_m \approx 0.28 \Gamma$  and  $\gamma_e \approx 4.7 \Gamma$ .)

In conclusion, we showed that a planar metamaterial array can be designed in such a way that the excitation energy is overwhelmingly dominated by a subradiant eigenmode that spatially extends over the large array. This is very different, e.g., from recent observations of subradiance [45] in an atomic vapor where only a very small fraction of the emitters was found to possess a suppressed decay rate. Our analysis of the controlled state preparation paves the way towards engineering complex correlated EM excitations that consist of large numbers of resonators, with potential applications, e.g., in light storage, optical memories, and light emission. The metamaterial resonator arrays also bear resemblance to other resonant emitter lattices, such as cold-atom systems [33,46–49], which similarly respond to light as classical oscillators in the typically applied low light intensity limit [29,30]. However, finding experimental evidence of correlated light-mediated interactions in atomic vapors is generally challenging [50], and correlated light excitations could therefore potentially be better utilized in metamaterial applications.

Following a period of embargo, the data presented in this Letter can be found at [51].

We acknowledge financial support from the EPSRC (Grants No. EP/G060363/1 and No. EP/M008797/1), the Leverhulme Trust, the Royal Society, and the MOE Singapore Grant No. MOE2011-T3-1-005. We also acknowledge the use of the IRIDIS High Performance Computing Facility at the University of Southampton.

---

[1] R. H. Dicke, *Phys. Rev.* **93**, 99 (1954).  
 [2] M. Gross and S. Haroche, *Phys. Rep.* **93**, 301 (1982).  
 [3] R. G. DeVoe and R. G. Brewer, *Phys. Rev. Lett.* **76**, 2049 (1996).  
 [4] C. Hettich, C. Schmitt, J. Zitzmann, S. Khn, I. Gerhardt, and V. Sandoghdar, *Science* **298**, 385 (2002).  
 [5] B. H. McGuyer, M. McDonald, G. Z. Iwata, M. G. Tarallo, W. Skomorowski, R. Moszynski, and T. Zelevinsky, *Nat. Phys.* **11**, 32 (2015).  
 [6] Y. Takasu, Y. Saito, Y. Takahashi, M. Borkowski, R. Ciuryło, and P. S. Julienne, *Phys. Rev. Lett.* **108**, 173002 (2012).  
 [7] E. Prodan, C. Radloff, N. J. Halas, and P. Nordlander, *Science* **302**, 419 (2003).  
 [8] N. Liu, L. Langguth, T. Weiss, J. Kästel, M. Fleischhauer, T. Pfau, and H. Giessen, *Nat. Mater.* **8**, 758 (2009).  
 [9] A. Lovera, B. Gallinet, P. Nordlander, and O. J. Martin, *ACS Nano* **7**, 4527 (2013).  
 [10] J. A. Fan, C. Wu, K. Bao, J. Bao, R. Bardhan, N. J. Halas, V. N. Manoharan, P. Nordlander, G. Shvets, and F. Capasso, *Science* **328**, 1135 (2010).

[11] M. Hentschel, D. Dregely, R. Vogelgesang, H. Giessen, and N. Liu, *ACS Nano* **5**, 2042 (2011).  
 [12] M. Frimmer, T. Coenen, and A. F. Koenderink, *Phys. Rev. Lett.* **108**, 077404 (2012).  
 [13] D. Dregely, M. Hentschel, and H. Giessen, *ACS Nano* **5**, 8202 (2011).  
 [14] D. W. Watson, S. D. Jenkins, J. Ruostekoski, V. A. Fedotov, and N. I. Zheludev, *Phys. Rev. B* **93**, 125420 (2016).  
 [15] B. Hopkins, A. N. Poddubny, A. E. Miroshnichenko, and Y. S. Kivshar, *Phys. Rev. A* **88**, 053819 (2013).  
 [16] C. Forestiere, L. Dal Negro, and G. Miano, *Phys. Rev. B* **88**, 155411 (2013).  
 [17] N. Papisimakis, V. A. Fedotov, Y. H. Fu, D. P. Tsai, and N. I. Zheludev, *Phys. Rev. B* **80**, 041102(R) (2009).  
 [18] V. A. Fedotov, N. Papisimakis, E. Plum, A. Bitzer, M. Walthers, P. Kuo, D. P. Tsai, and N. I. Zheludev, *Phys. Rev. Lett.* **104**, 223901 (2010).  
 [19] T. Holstein, *Phys. Rev.* **72**, 1212 (1947).  
 [20] F. W. Cummings, *Phys. Rev. A* **33**, 1683 (1986).  
 [21] N. I. Zheludev, S. L. Prosvirnin, N. Papisimakis, and V. A. Fedotov, *Nat. Photonics* **2**, 351 (2008).  
 [22] G. Adamo, J. Y. Ou, J. K. So, S. D. Jenkins, F. De Angelis, K. F. MacDonald, E. Di Fabrizio, J. Ruostekoski, and N. I. Zheludev, *Phys. Rev. Lett.* **109**, 217401 (2012).  
 [23] S. D. Jenkins and J. Ruostekoski, *Phys. Rev. Lett.* **111**, 147401 (2013).  
 [24] F. Lemoult, G. Lerosey, J. de Rosny, and M. Fink, *Phys. Rev. Lett.* **104**, 203901 (2010).  
 [25] S. Linden, F. B. P. Niesler, J. Förstner, Y. Grynko, T. Meier, and M. Wegener, *Phys. Rev. Lett.* **109**, 015502 (2012).  
 [26] V. A. Fedotov, M. Rose, S. L. Prosvirnin, N. Papisimakis, and N. I. Zheludev, *Phys. Rev. Lett.* **99**, 147401 (2007).  
 [27] See Supplemental Material <http://link.aps.org/supplemental/10.1103/PhysRevLett.119.053901> for additional details regarding technical background information, which includes Refs. [8,28–37].  
 [28] F. Nissen, J. M. Fink, J. A. Mlynek, A. Wallraff, and J. Keeling, *Phys. Rev. Lett.* **110**, 203602 (2013).  
 [29] J. Ruostekoski and J. Javanainen, *Phys. Rev. A* **55**, 513 (1997).  
 [30] M. D. Lee, S. D. Jenkins, and J. Ruostekoski, *Phys. Rev. A* **93**, 063803 (2016).  
 [31] S. D. Jenkins and J. Ruostekoski, *Phys. Rev. B* **86**, 085116 (2012).  
 [32] H. Kuwata, H. Tamaru, K. Esumi, and K. Miyano, *Appl. Phys. Lett.* **83**, 4625 (2003).  
 [33] S. D. Jenkins and J. Ruostekoski, *Phys. Rev. A* **86**, 031602 (R) (2012).  
 [34] J. D. Jackson, *Classical Electrodynamics*, 3rd ed. (Wiley, New York, 1999).  
 [35] A. A. Svidzinsky, J.-T. Chang, and M. O. Scully, *Phys. Rev. A* **81**, 053821 (2010).  
 [36] J. Javanainen, J. Ruostekoski, B. Vestergaard, and M. R. Francis, *Phys. Rev. A* **59**, 649 (1999).  
 [37] M. Hebenstreit, B. Kraus, L. Ostermann, and H. Ritsch, *Phys. Rev. Lett.* **118**, 143602 (2017).  
 [38] A. Ishimaru, *Wave Propagation and Scattering in Random Media: Multiple Scattering, Turbulence, Rough Surfaces*,

- and Remote Sensing* (Academic Press, St. Louis, Missouri, 1978), Vol. 2.
- [39] O. Morice, Y. Castin, and J. Dalibard, *Phys. Rev. A* **51**, 3896 (1995).
- [40] D. S. Wiersma, M. P. van Albada, B. A. van Tiggelen, and A. Lagendijk, *Phys. Rev. Lett.* **74**, 4193 (1995).
- [41] J. Javanainen, J. Ruostekoski, Y. Li, and S.-M. Yoo, *Phys. Rev. Lett.* **112**, 113603 (2014).
- [42] J. Javanainen and J. Ruostekoski, *Opt. Express* **24**, 993 (2016).
- [43] S. Savo, N. Pappasimakis, and N. I. Zheludev, *Phys. Rev. B* **85**, 121104(R) (2012).
- [44] M. Fleischhauer, A. Imamoglu, and J. P. Marangos, *Rev. Mod. Phys.* **77**, 633 (2005).
- [45] W. Guerin, M. O. Araújo, and R. Kaiser, *Phys. Rev. Lett.* **116**, 083601 (2016).
- [46] R. J. Bettles, S. A. Gardiner, and C. S. Adams, *Phys. Rev. A* **92**, 063822 (2015).
- [47] S.-M. Yoo and S. M. Paik, *Opt. Express* **24**, 2156 (2016).
- [48] G. Facchinetti, S. D. Jenkins, and J. Ruostekoski, *Phys. Rev. Lett.* **117**, 243601 (2016).
- [49] E. Shahmoon, D. S. Wild, M. D. Lukin, and S. F. Yelin, *Phys. Rev. Lett.* **118**, 113601 (2017).
- [50] S. Jennewein, M. Besbes, N. J. Schilder, S. D. Jenkins, C. Sauvan, J. Ruostekoski, J.-J. Greffet, Y. R. P. Sortais, and A. Browaeys, *Phys. Rev. Lett.* **116**, 233601 (2016).
- [51] <http://doi.org/10.5258/SOTON/D0155>.